Vibrational and electronic structure of the $3d^{-1} \rightarrow 4p(\pi,\sigma)^{-2}$ normal Auger spectrum of HBr studied by fully relativistic configuration-interaction calculations

T. Matila,[1] K. Ellingsen,[2] T. Saue,[3] H. Aksela,[1] and O. Gropen[2]
[1]*Department of Physical Sciences, University of Oulu, PL 3000, FIN-90401 Oulu, Finland*
[2]*Institute of Mathematical and Physical Sciences, University of Tromsø, N-9037, Tromsø, Norway*
[3]*Laboratoire de Physique Quantique, IRSAMC, Université Paul Sabatier, 118 route de Narbonne, 31062 Toulouse Cedex 4, France*
(Received 1 June 1999; published 15 February 2000)

Fully relativistic, self-consistent field calculations, based on the Dirac-Coulomb-Gaunt Hamiltonian, were performed on the ground state of HBr, the Br $3d$–ionized HBr^+, and the $4p(\pi,\sigma)^{-2}$ states of HBr^{2+}. Correlation in the ground and valence-excited states and partially in the Br $3d$ ionized states was described using a configuration-interaction (CI) method. Calculated ionization energies and bond lengths were found to be in good agreement with recent experimental results. The distortion in the vibrational bands of the $3d^{-1} \rightarrow 4p\pi^{-2}$ Auger transitions due to lifetime vibrational interference was verified through *ab initio* calculations. Bands due to the transitions to bound and continuum vibrational states of the same electronic state were reproduced by calculations and compared with experimentally determined profiles. The nonadiabatic effects in the spin-orbit-induced avoided level crossing were investigated using adiabatic and diabatic electronic basis sets.

PACS number(s): 32.80.Hd, 31.10.+z, 31.30.Jv, 33.70.−w

I. INTRODUCTION

Progress in experimentation has allowed us to resolve the molecular field and vibrational splittings of the core-hole states and to detect the combined effect of intermediate and final states to the fine structure of Auger electron spectra (AES). Molecules containing heavy element(s) are cases where the assignment of these features, usually based on the assumption of the similarity of elements with similar outer shell structure, easily fails. For instance, in HF, HCl, HBr, and HI, the AES where the similar valence orbitals are involved in the decay, differ greatly from each other. This is related to the fact that the intensity distribution of the AES depends on the character of the intermediate state—of the $1s_F$, $2p_{Cl}$, $3d_{Br}$, $4d_I$ core-hole state in the above examples—and its match with the valence charge distribution involved in the decay (see, e.g., [1] and references therein).

For a theoretical description of the core-hole states, both the molecular field and spin-orbit interaction need to be included on the same footing. The recent results by Ellingsen *et al.* [2] indicated that relativistic effects are of importance in molecules as light as HCl when highly excited states are involved. In heavier molecules as in HBr, the relativistic effects, especially the spin-orbit interaction, are of importance also in the valence doubly-ionized states, the final states of the Auger decay. Relativistic molecular calculations are a natural choice for predicting the properties of such states. However, it should be remembered that in the final states the correlation effects are even more important, and a relativistic method including correlation treatment should be employed.

In this paper we present results of fully relativistic calculations for the adiabatic potential energy curves of the ground state of HBr, the Br $3d$–ionized, molecular-field-split states of HBr^+ and the $4p(\sigma,\pi)^{-2}$ states of HBr^{2+}. In $\Lambda\Sigma$ coupling the manifold of double-$4p(\sigma,\pi)$–ionized HBr states splits into three classes according to the distribution of the two holes. If both holes are in the bonding $4p\sigma$ orbitals a strongly repulsive $^1\Sigma^+$ electronic state is obtained. The mixed $\sigma^{-1}\pi^{-1}$ states ($^3\Pi$ and $^1\Pi$) are dissociative as well. On the other hand, the $^3\Sigma^-$, $^1\Delta$, and $^1\Sigma^+$ states arising from placing both holes in the nonbonding $4p\pi$ orbitals are expected to be bound. The triplets are further split into $^3\Sigma^-_{1,0+}$ and $^3\Pi_{0-,0+,1,2}$ due to spin-orbit interaction.

As demonstrated by Pahl *et al.* in the case of HF [3], the nonadiabatic effects may be important in AES. Thus, we also approximate the diabatic potential curves for the $4p\pi^{-2}(^1\Sigma^+_{0-})$ and $4p\sigma^{-1}\pi^{-1}(^3\Pi_{0-})$ states of HBr^{2+}. The potential curves were further used in calculating the vibrational structure of the AES.

The results of the calculations are directly compared to the experimental values obtained by Püttner *et al.* [1]. Especially the experimentally observed distortion in the vibrational bands of the $3d^{-1} \rightarrow 4p\pi^{-2}$ Auger transitions due to lifetime vibrational interference is verified by calculations. (For a detailed theoretical description of the lifetime vibrational effects, see Ref. [4].) The results of this work are also compared to the calculations performed by Banichevich *et al.* [5] who included scalar relativistic (the mass velocity and Darwin terms) effects in the Hamiltonian. They treated the spin-orbit interaction as a perturbation causing predissociation of the nonrelativistically stable states.

In Sec. II we describe briefly the methods used in the calculations for the adiabatic potential energy curves, vibrational energies, and wave functions. The results of these calculations are further compared to recent experimental results. In Sec. III we investigate in more detail the lifetime interference effects and the nonadiabatic effects caused by spin-orbit interactions on the AES of HBr. These sections are followed by a conclusion.

TABLE I. The used RAS spaces in calculations for the ground state, Br $3d$−ionized, and doubly-valence-ionized HBr.

State	RAS1	RAS2	RAS3
Ground state	$4s\sigma$, $4p(\sigma,\pi)$		Virtual spinors
$3d^{-1}$		$3d$, $4s\sigma$, $4p(\sigma,\pi)$	Virtual spinors
$4p(\sigma,\pi)^{-2}$	$4s\sigma$	$4p(\sigma,\pi)$	Virtual spinors

II. COMPUTATION OF THE ADIABATIC POTENTIAL ENERGY CURVES, VIBRATIONAL ENERGIES, AND WAVE FUNCTIONS

A. Computational details

All calculations for the adiabatic potential curves were performed using the four-component relativistic *ab initio* MOLFDIR [6] program package. The nuclei were represented by a finite-nucleus model, i.e., a Gaussian charge distribution, with an exponential value of $2.413\,016\times10^{9}$ for Br.

The calculations were carried out in C_{4v} double-group symmetry. The C_{4v} is the highest subgroup of the $C_{\infty v}$, which can be exploited by the MOLFDIR program package. The two-electron interaction was described by treating both the Couloumb and Gaunt operators variationally for the ground state and the $4p(\sigma,\pi)^{-2}$ states. In calculating the $3d^{-1}$ states the number of integrals was heavily truncated in order to keep the computing time tolerable. The integrals between small components $[(SS|SS)$ integrals] as well as Gaunt integrals were not calculated at all.

Molecular spinors were generated by the Dirac-Hartree-Fock (DHF) method. The open-shell states were treated by an average of configurations formalism. For the $3d^{-1}$ states five electrons were averaged over the molecular-field-split components $3d_{3/2,3/2}$, $3d_{5/2,3/2}$, and $3d_{5/2,5/2}$ in the $\omega\omega$-coupled notation and for the $4p(\sigma,\pi)^{-2}$ states four electrons were averaged over the $4p\sigma$ and $4p\pi$ spinors. The different electronic states arising from the open-shell manifold were then resolved by a subsequent full CI within the open-shell spinor space. Correlation effects were studied using the restricted-active-space configuration-interaction (RASCI) method [7]. In the calculations of the ground state and the $4p(\sigma,\pi)^{-2}$ states, the electrons in the $4s\sigma$ and $4p(\sigma,\pi)$ spinors were correlated and for $3d^{-1}$ states, electrons in the $3d$ were correlated as well. The RAS spaces were defined as shown in Table I. All excitations from the RAS1 to RAS2 subspaces, all excitations within the RAS2 and single and double excitations from these spaces to RAS3 were allowed, leading to a multireference (MR) description of the $3d^{-1}$ and $4p(\sigma,\pi)^{-2}$ states. Virtual spinors with energies above 4 a.u. were deleted.

The generally contracted Gaussian basis sets used in this work are summarized in Table II. For bromine a primitive, nonrelativistic $16s13p8d$ basis, of Fægri [8] was reoptimized to a dual family basis, where the d exponents are a subset of the s exponents. This basis was augmented with a tight p exponent to improve the description of the $2p$ spin-orbital splitting. The basis set was then further increased to better describe correlation and polarization. The final $18s16p10d2f$ large component basis was subjected to a general contraction in the pattern $[4s+4,6p+5,2d+4,2]$, meaning that four s-functions, five p-functions, two d-functions, and two f-functions were kept uncontracted to keep the flexibility in the basis set. For the large components of hydrogen a $6s3p1d$ primitive basis with exponents from Dunning [9] was used. The basis was generally contracted to a $[3s+3,3,1]$ pattern. Basis sets for the small components were generated by the atomic balance relation [10].

Vibrational energies and wave functions were calculated by numerical integration of the nuclear Schrödinger equation in the standard manner (Numerov scheme), the potentials of the quasibound states being truncated at the top of the barrier in order to ensure stable solutions for a bound state. The spline fit was applied to calculated points. A large number of orthonormal vibrational continuum wave functions were calculated for the simulations of the bound-continuum transitions (see Sec. III for details). We have neglected rotational degrees of motion in all calculations.

In the relativistic scheme we work with intermediate coupling where only the ω and Ω quantum numbers are feasible. We have, however, used the conventional nonrelativistic notations to describe the $4p(\pi,\sigma)^{-2}$ states of HBr^{2+}. The notations used are valid only in the relatively small internuclear distances $R<1.5$ Å; at longer bond lengths some states completely change their character due to spin-orbit coupling.

B. Results and comparison with experiment and previous calculations

1. Details of previous experiments

In the recent work by Püttner *et al.* [1] as well as in the prior work by Wannberg *et al.* [11] only the four lowest final

TABLE II. Basis sets.

	Large components		Small components	
	Primitive basis	Contracted basis	Primitive basis	Contracted basis
Br basis	$18s16p10d2f$	$4s+4,6p+5,2d+4,2$	$16s18p16d10f2g$	$3s+5,5p+5,6d+5,2f+4,2$
H basis	$6s3p1d$	$3s+3,3,1$	$3s7p3d1f$	$3,3p+4,3,1$

TABLE III. Experimental [12,13,1] and calculated bond lengths for the ground state, Br $3d$−ionized, and doubly-valence-ionized HBr^{2+}.

State	Expt. [12,13,1]	Dirac-Fock	MR-CI	Nonrelativistic [5]
		R_e (Å)		
Ground state	1.414	1.404	1.413	1.41
$3d^{-1}$	1.450	1.427	1.445	
$4p\pi^{-2}(^3\Sigma^-_{0+,1})$	1.563	1.524	1.542	1.55(1.49)
$4p\pi^{-2}(^1\Delta_2)$	1.560	1.524	1.541	1.54(1.49)
$4p\pi^{-2}(^1\Sigma_0)$	1.581	1.527	1.559	1.55(1.50)
$4p\sigma^{-1}\pi^{-1}(^3\Pi_2)$		2.047	2.212	
$4p\sigma^{-1}\pi^{-1}(^3\Pi_{0-})$		1.719	1.833	

states arising from $4p\pi^{-2}$ were clearly resolved in the experimental AES. The remaining final states are dominated by transitions to vibrational continuum giving rise to broad spectral features. Thus the quality of calculated bond lengths as well as binding energies for the spin-orbit-split $^3\Pi$ states and the $^1\Pi_1$ state cannot be tested due to the lack of experimental data.

The experimental results, excluding ground-state values, are taken from the work by Püttner *et al.* [1]. They included the vibrational lifetime interference when fitting the data but calculated the vibrational matrix elements by assuming Morse potentials for the ground state, the intermediate $3d^{-1}$ core-hole state, and the $4p\pi^{-2}$ final states. For the $3d^{-1}$ core-hole state they assumed equal potential energy curves for all molecular-field-split components. The values for the potential energy surface of the ground state and the $3d^{-1}$ state were taken from literature [12] and recent photoemission spectra [13], respectively. The value for the lifetime width of $\Gamma = 95$ meV was taken from photoabsorption spectra [14]. The reliability of the fitting procedure used in the experimental analysis [1] is discussed later in this paper.

2. Ground state

The optimized bond lengths and vibrational constants for the ground state are presented in Tables III and IV, respectively, together with the experimental values [12]. The DHF bond distance is 0.01 Å shorter than the experimental bond length. At the CI level the calculated bond length is only 0.001 Å shorter than the experimental value. The calculated bond lengths as well as vibrational constants are well in line with the results by Visscher, Styszyñski, and Nieuwpoort [15], who used slightly smaller basis sets.

3. Br 3d−ionized states

In $\omega\omega$ coupling the manifold of Br $3d$−ionized states spans five states ($\Omega = 1/2,3/2,1/2,3/2,5/2$). We were not able to converge the $\Omega = 1/2$ states at the DHF level, so the results reported here are restricted to the remaining three states. A further complication is the large number of orbitals correlated at the CI level [$3d,4s\sigma,4p(\sigma,\pi)$]. This lead to very severe size-consistency errors already with a moderately small number of virtual orbitals included in RAS3, the corrections of Langhoff and Davidson [16] giving rise to drastic, clearly erroneus, changes in energy splittings between the molecular-field-split states.

The calculated bond lengths and vibrational constants for the Br $3d$-ionized HBr are given in Tables III and IV, respectively. Note that the determination of the experimental value [13] was based on the assumption that the potential energy functions are similar for all spin-orbit and molecular-field-split components. The calculated bond length is obtained as an average of the molecular-field-split components $3d_{3/2,3/2}$, $3d_{5/2,3/2}$, and $3d_{5/2,5/2}$ in the $\omega\omega$-coupled notation. This average represents all of these three states well, the largest deviations from the average being only 0.002 Å. The increase in the bond length relative to ground state is too small at the DHF level (0.023 Å) as compared with experiment. The increase of 0.032 Å on the CI level is within the accuracy of experimental results [13]. The vibrational energies and wave functions were calculated using the average potential of these spinors.

4. Valence ionized HBr^{2+}

The calculated and experimentally determined potential energy curves for the $4p\pi^{-2}$ states and the calculated curves

TABLE IV. Experimental [12,13,1] and calculated vibrational constants for the ground state, Br $3d$−ionized, and doubly-valence-ionized HBr^{2+}.

State	Expt. [12,13,1]	Dirac-Fock	MR-CI
		$\hbar\omega$, x$\hbar\omega$ (meV)	
Ground state	328.2, 5.6	344, 4.4	333, 4.8
$3d^{-1}$	315	322, 6.2	
$4p\pi^{-2}(^3\Sigma^-_{0+,1})$	218, 8.8	247, 11.6	235, 8.7
$4p\pi^{-2}(^1\Delta_2)$	220, 9.9	250, 19.8	240, 11.6

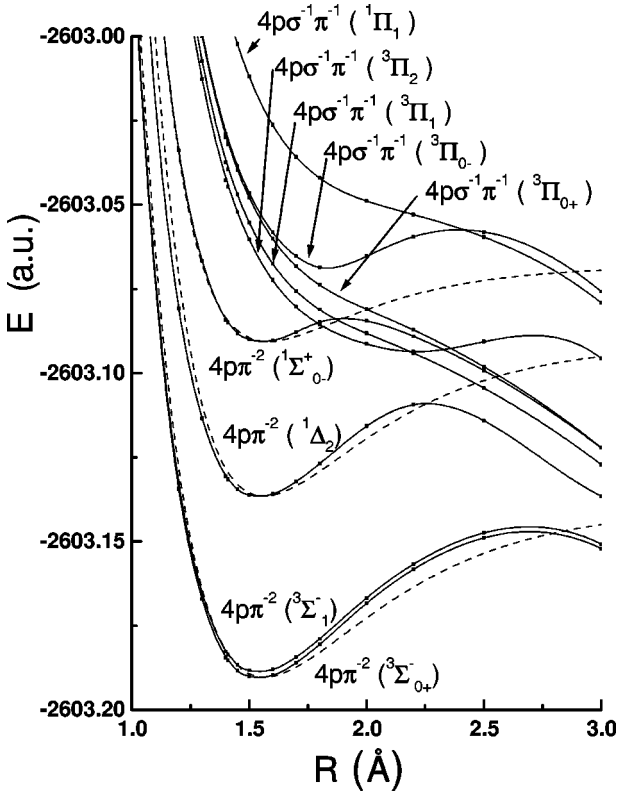

FIG. 1. Potential energy curves for the $4p\pi^{-2}$ and $4p\sigma^{-1}\pi^{-1}$ states of HBr^{2+} calculated by the MR-CI method. The dashed lines correspond to Morse potentials extracted from the experimental vibrational constants by Püttner *et al.* [1].

for the $4p\sigma^{-1}\pi^{-1}$ states of HBr^{2+} are presented in Fig. 1. The highest excited state $4p\sigma^{-2}(^1\Sigma^+_{0-})$, is strongly repulsive, and is not shown in Fig. 1.

The nonrelativistic double-hole states of AES are perturbed by spin-orbit coupling. In particular, spin-orbit interaction between the dissociative $^3\Pi_{0-}$ state and the bonding $^1\Sigma^+_{0-}$ state leads to an avoided crossing as clearly seen in Fig. 1. The 0+ component of $^3\Pi$ does not interact with other states through spin-orbit coupling and therefore represents the unperturbed state, a feature that is exploited in the calculation of the vibrational band profiles in Sec. III B. An avoided crossing takes place also between the $^3\Pi_2$ and $^1\Delta_2$ states, but at longer bond lengths, and should therefore influence the AES to a lesser degree.

Experimental and calculated bond lengths for the valence-excited states of HBr^{2+} are given in Table III. The DHF bond lengths for these states are generally too small as compared with experimental values. The CI values are in better agreement being about 0.02 Å shorter than the experimental values. The small variation in the relative distances between the bond lengths of the $4p\pi^{-2}$ states is well predicted by theory.

The calculated and experimental binding energies are given in Table V. The DHF binding energies are in general too small and energy splittings between $^3\Sigma^-_{0+,1}$, $^1\Delta_2$, and $^1\Sigma^+_{0-}$ are too large as compared with experiment. The CI energies are slightly too high. The nonrelativistic values for binding energies by Banichevich *et al.* [5] seem to be in better agreement with experimental results. They have, however, been corrected with respect to experimental results. The splittings predicted by relativistic CI calculations are in general in slightly better agreement with experiment than the splittings obtained by the nonrelativistic calculations [5]. The small splitting (about 50 meV) between the $\Omega=0$ and $\Omega=1$ states of $^3\Sigma^-$ is well reproduced by the DHF and CI calculations.

The bromine $3d$ manifold was correlated only for the Br $3d$–ionized states. The effect of this core-valence correlation for the other states was studied by investigating the Br^- and Br^+ asymptotes, assuming it to be a purely atomic effect. A small shift downwards of about 0.015 eV in binding energies for valence-ionized HBr^{2+} was observed when the correlation energies between the ground state of Br^- and the different states belonging to Br^+ were compared.

The number of quasistable vibrational levels for the $4p\pi^{-2}$ states is heavily reduced by the avoided crossings caused by spin-orbit coupling. This rather strong effect is clearly visible in the potential energy curves presented in Fig. 1. For the $^3\Sigma^-_{0+,1}$ states we found six stable vibrational states at the DHF level and seven at the CI level. For $^1\Delta_2$ the numbers at the DHF and CI level were found to be three and four, and for $^1\Sigma^+_{0-}$, zero and one, respectively. When these values from the adiabatic approximation are compared to the

TABLE V. Experimental [1] and calculated binding energies (E_B) of doubly-ionized HBr^{2+}.

State	ν	Expt. [1]	Dirac-Fock	MR-CI	Nonrelativistic [5]
			E_B (eV)		
$4p\pi^{-2}(^3\Sigma^-_{0+,1})$	0	32.581, 32.636	30.556, 30.602	33.082, 33.130	32.30
	1	32.783, 32.838	30.779, 30.825	33.298, 33.346	32.52
	2	32.968, 33.023	30.981, 31.027	33.500, 33.548	32.72
$4p\pi^{-2}(^1\Delta_2)$	0	33.940	32.235	34.547	33.92
	1	34.143	32.446	34.761	34.14
	2	34.329	32.617	34.957	34.35
$4p\pi^{-2}(^1\Sigma_0)$	0	35.205	(33.497)	35.779	34.87
$4p\sigma^{-1}\pi^{-1}(^3\Pi_2)$	0		33.040	35.648	
$4p\sigma^{-1}\pi^{-1}(^3\Pi_{0-})$	0		34.028	36.365	

results by Banichevich *et al.* [5], who found eight, seven, and seven states for $^3\Sigma^-$, $^1\Delta$, and $^1\Sigma^+$, respectively, the number of vibrational states is clearly seen to be reduced. This finding, however, agrees in essence with results of Banichevich *et al.*, who found considerably large lifetime widths of 219 and 165 meV for $\nu=5$ state of $^1\Delta$ and $\nu=2$ state of $^1\Sigma^+$, respectively. In addition, due to the spin-orbit interaction two of the $^3\Pi$ states ($\Omega=0-,2$) possess minima, in slightly longer internuclear distances than the states arising from the $4p\pi^{-2}$ configurations. The state assigned as $^3\Pi_{0-}$ is actually more of $^1\Sigma^+_{0-}$ character at longer internuclear distances, and the state assigned as $^3\Pi_2$ is actually more of $^1\Delta_2$.

The experimental results [1], obtained using Morse potentials, cannot be used to confirm the findings. More realistic potentials, especially for the $^1\Sigma^+$, are needed in the data analysis to make a final conclusion of the number and nature of the vibrational levels.

The vibrational energy splittings can be deduced from Table IV. The binding energies for the lowest vibrational states are given in Table V. The nonrelativistic [5] and relativistic values, of about the same calculational quality, for the lowest states are very similar. In general, discrepancies between experimental and calculated vibrational splittings are very small.

III. LIFETIME INTERFERENCE AND NONADIABATIC EFFECTS IN THE AUGER ELECTRON SPECTRUM OF HBR

A. Lifetime interference using the adiabatic approximation

In the experimental work of Püttner *et al.* [1] the vibrational lifetime interference was shown to have a significant influence on the AES of HBr. For a detailed comparison between experiment and theory, we calculated the vibrational band structures using parameters obtained from our calculations. Unfortunately, we were not able to calculate electronic transitions amplitudes. We included one electronic intermediate state only and used the experimental value for lifetime width $\Gamma=95$ meV for the Br $3d$ core-hole state taken from photoabsorption spectra [14]. This means that we are working in the ''constant resonant width approximation'' [17]. In reality the lifetime width may vary depending both on the intermediate state and on the internuclear distance. This is in particular true in the presence of avoided level crossings, where the adiabatic Born-Oppenheimer approximation is no longer valid.

For $^3\Sigma^-_{0+}$ and $^1\Delta_2$ we calculated the vibrational matrix elements using the numerical vibrational wave functions that were obtained by solving the nuclear Schrödinger equation using the adiabatic electronic basis. Thereafter the vibrational band profiles were calculated from the interference formula given by Correia *et al.* [17] (their Eq. (5); see also Ref. [4]). We also compared our calculated profiles to the ones obtained by using the experimentally determined Morse potential by Püttner *et al.* [1]. The resulting profiles are presented in Fig. 2. The distortion caused by postcollision interaction (PCI) was not included in the simulations. The vibrational band profiles for the $^3\Sigma^-_{0+}$ and $^1\Delta_2$ states are very similar. Especially the shoulder in the high-kinetic-energy side is very well predicted by present calculations verifying the reassignment by Püttner *et al.* [1] of this feature as being the interference contribution instead of the hot band. The intensity of the highest peaks is in both peaks slightly overestimated by calculations as compared with experiment. The transitions to vibrational continuum for the $^3\Sigma^-_{0+}$ are almost negligible and are hardly visible in the experimental spectrum. The shape of the $^3\Sigma^-_1$ band (not shown) is almost identical to that of the $^3\Sigma^-_{0+}$. An avoided crossing observed involving the $^3\Pi_2$ and $^1\Delta_2$ states causes a small increase of continuum transitions for $^1\Delta_2$. The crossing, however, is at long bond distance and does not influence the AES significantly. Our calculations verify the validity of the Morse potential fitting procedure used for the treatment of these states in the experimental spectra.

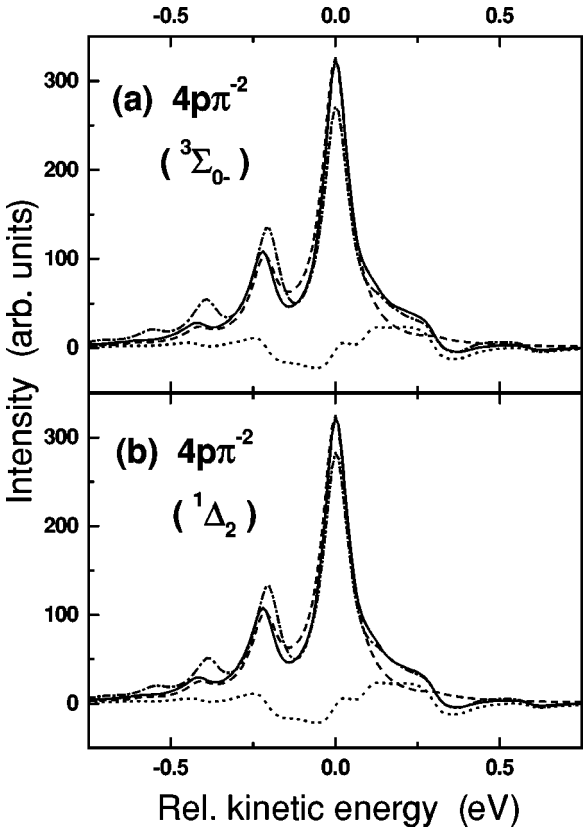

FIG. 2. Calculated and experimental vibrational band profiles for the (hypothetical) $3d^{-1}$-$4p\pi^{-2}$ ($^3\Sigma^-_{0+}$ and $^1\Delta_2$) transitions. The solid lines correspond to MR-RASCI calculations. The dashed lines correspond to direct term in the formula by Correia *et al.* [17] whereas the dotted lines represent the interference term. The dash-dotted lines correspond to results by Püttner *et al.* [1]. The kinetic energies of Auger electron are given relative to 0-0-0 vibrational transition.

B. Nonadiabatic effects

The spin-orbit-induced avoided crossing between $^1\Sigma^+_{0-}$ and $^3\Pi_{0-}$ causes significant effects in the AES. In this case the avoided level crossing is in the Franck-Condon region

and changes in the spectral features are expected. One must note that calculations predict only one quasibound vibrational state for the $^1\Sigma^+_{0-}$ state, the continuum band closely resembling one or more transitions to stable vibrational states. Therefore, in an experimental spectrum with moderate statistics [1], the fit with Morse potential may look reasonable. The DHF calculation predicts no stable vibrational states for this state, thus highlighting the importance of the correlation treatment.

Due to the presence of strong nonadiabatic effects in the final Auger states, we have modified the interference formula given by Correia *et al.* [17] to take these effects into account. The potential curves represented in Fig. 1 are adiabatic potential curves, the points at each internuclear distance given by the eigenvalue spectrum of the electronic Hamiltonian. In this particular case two states, $^1\Sigma^+_{0-}$ and $^3\Pi_{0-}$, interact through the spin-orbit part $\hat{H}_{SO}$ of this operator. Accordingly, the unperturbed states are eigenfunctions of the remaining spin-free part $\hat{H}_{sf}$ of the electronic Hamiltonian. The specific forms of the $\hat{H}_{sf}$ and $\hat{H}_{SO}$ operators need not concern us here, but within a four-component relativistic formalism they would correspond to the separation proposed by Dyall [18]. The points of the two potential curves in question can be thought of as resulting from diagonalizing the 2×2 Hamiltonian matrix in the basis of the unperturbed $^3\Pi_{0-}$ and $^1\Sigma^+_{0-}$ states. The $^3\Pi_{0+}$ state does not couple to other states through spin-orbit interaction, and its potential curve therefore corresponds to that of the unperturbed $^3\Pi_{0-}$ state. From the energies of adiabatic $^1\Sigma^+_{0-}$ and $^3\Pi_{0-}$ and from the energy of $^3\Pi_{0+}$, the energy of the unperturbed $^1\Sigma^+_{0-}$ state is easily found since the trace of any matrix is conserved under a unitary transformation. Likewise the off-diagonal spin-orbit coupling elements as a function of internuclear distance are straightforwardly calculated.

The calculated (MR-RASCI) off-diagonal spin-orbit-coupling elements as a function of internuclear distance as well as diabatic and adiabatic potential energy curves for $^3\Pi_{0-}$ and $^1\Sigma^+_{0-}$ states are presented in Fig. 3. The resulting potential curves of the unperturbed states are smooth functions of the internuclear distance, so that the nonadiabatic coupling elements, which include the gradients of electronic wave functions with respect to nuclear coordinates, are small and can be neglected. Accordingly the unperturbed $^3\Pi_{0-}$ and $^1\Sigma^+_{0-}$ states form a diabatic electronic basis, and transition moments may be approximated by nonrelativistic values.

The final Auger states are eigenfunctions of the molecular Hamiltonian that can be written as $\hat{H}=\hat{T}_N+\hat{H}_{sf}+\hat{H}_{SO}$ where $\hat{T}_N$ is the kinetic energy operator of the nuclei. Approximate solutions can be found variationally by diagonalizing the Hamiltonian matrix in the basis $\{|^1\Sigma^+_{0-}(\vec{r};\vec{R})\rangle|\chi_i(\vec{R})\rangle\}\cup\{|^3\Pi_{0-}(\vec{r};\vec{R})\rangle|\chi_j(\vec{R})\rangle\}$. Here $|^1\Sigma^+_{0-}(\vec{r};\vec{R})\rangle$ and $|^3\Pi_{0-}(\vec{r};\vec{R})\rangle$ represent the electronic wave functions of the unperturbed states and $|\chi_i(\vec{R})\rangle$ and $|\chi_j(\vec{R})\rangle$ their respective vibrational wave functions. The latter are found by solving the vibrational equations for the unperturbed $^1\Sigma^+_{0-}$ and $^3\Pi_{0-}$ states separately

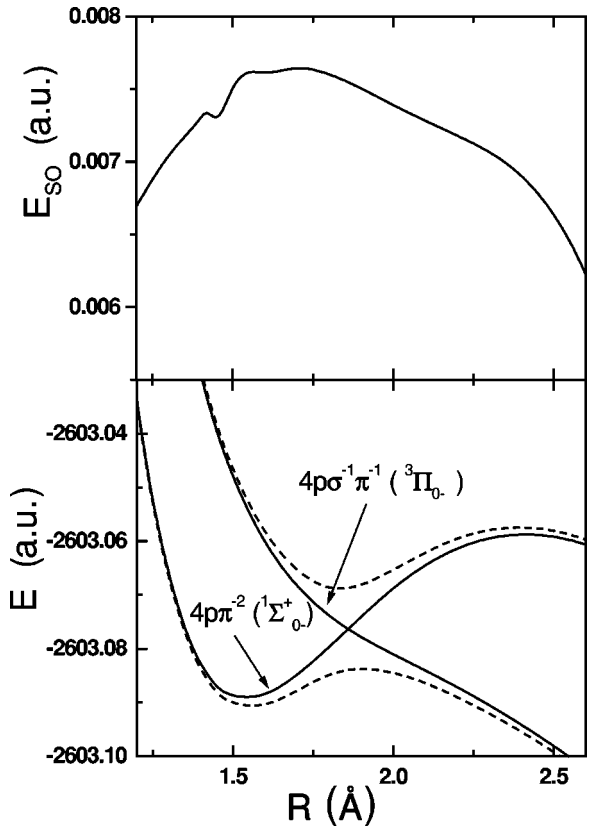

FIG. 3. Calculated (MR-CI) off-diagonal spin-orbit-coupling element E_{SO} as a function of internuclear distance, diabatic and adiabatic potential energy curves for the $^3\Pi_{0-}$ and $^1\Sigma^+_{0-}$ states. The solid lines in the figure below correspond to diabatic potential energy curves, whereas the dashed lines correspond to adiabatic potential energy curves.

$$[\hat{T}_N+E_{sf}(\vec{R})]\chi_k(\vec{R})=E\chi_k(\vec{R}). \tag{1}$$

If we assume that the gradients of electronic wave functions with respect to nuclear coordinates vanish, the only nondiagonal matrix elements in the Hamiltonian matrix are the spin-orbit integrals of type

$$\int d\vec{R}\chi_i(\vec{R})E_{SO}(\vec{R})\chi_j(\vec{R}), \tag{2}$$

where

$$E_{SO}(\vec{R})=\langle{}^1\Sigma^+_{0-}(\vec{r};\vec{R})|\hat{H}_{SO}|^3\Pi_{0-}(\vec{r};\vec{R})\rangle, \tag{3}$$

which involve only values that we have already extracted from adiabatic and diabatic potential curves.

Although we were not able to calculate electronic transition amplitudes, we made simulations to demonstrate how the spin-orbit interaction may cause differences in the AES. In all simulations we assumed the same magnitude for all transition moments. See Figs. 4(a)–4(d). The simulation 4(a) refers to calculation using the adiabatic basis set, 4(b) refers to the diabatic calculation with $\hat{H}_{SO}$ not included in the mo-

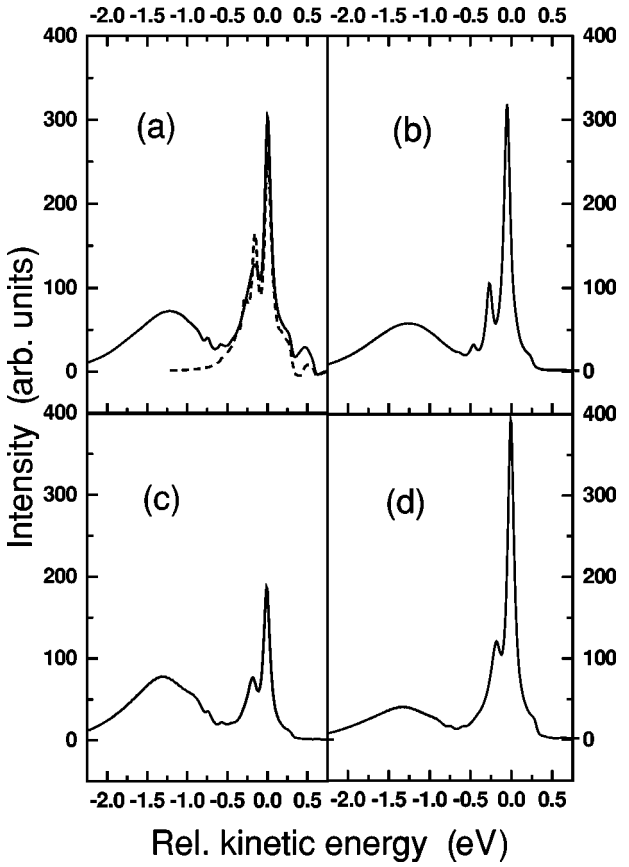

FIG. 4. Calculated and experimental vibrational band profile for the (hypothetical) $3d^{-1}$-$4p\pi^{-2}(^1\Sigma^+_{0-})$, $4p\pi^{-1}\sigma^{-1}$ $(^3\Pi_{0-})$ transition. The solid lines correspond to calculations described in the text. The dashed line corresponds to the spectrum generated from the vibrational constants obtained by Püttner *et al.* [1]. For details, see the text.

lecular Hamiltonian. The calculations 4(c) and 4(d) refer to variational-type calculations described above. In calculation 4(c) the transtions moments for $^3\Pi_{0-}$ and $^1\Sigma^+_{0-}$ are assumed to have the same sign, whereas in the calculation 4(d) the signs are assumed to be different. The straightforward copying of the signs from atomic calculations is not possible, because even though the atomic Auger transition to the $^1S_0$ state comes mainly from one channel, the transition to the atomic triplet state comes from various channels with different signs depending on the spatial orientation, i.e., orbital angular momentum quatum numbers of the continuum electron. The simulations in Figs. 4(a)–4(d) are presented together with the ''experimental'' spectrum for the $^1\Sigma^+_{0-}$ obtained with similar computations but with the vibrational constants taken from Püttner *et al.* [1].

The different methods lead to significantly unlike spectra. The calculation of Fig. 4(b) represents the case where we have completely neglected the spin-orbit interaction. In this case the spectrum consists of a clean vibrational progression caused by the bonding $^1\Sigma^+_{0-}$ and a broad, Gaussian type $^3\Pi_{0-}$ band caused by transitions to vibrational continuum.

In Fig. 4(a), the adiabatic approximation and the predicted interference contributions are very strong. This feature, which may be an artifact, originates from the fact that the vibrational bound state of $^1\Sigma^+_{0-}$ is close to the dissociation limit, and thus energetically close to vibrational continuum. The calculations of Figs. 4(c) and of 4(d) predict only small interference contributions. The weaker interference structure arises because now the continuum states close to the bound states of $^1\Sigma^+_{0-}$ are mainly associated to $^3\Pi_{0-}$ and thus interact only by means of a spin-orbit interaction. The clear indication of the effects of the spin-orbit interaction is the strong variation of the relative magnitudes between sharp peaks and continuum bands. If the signs of the Coulomb transition moments are the same [calculation 4(c)] we notice that the broad $^3\Pi_{0-}$ band enhances and the $^1\Sigma^+_{0-}$ peaks, in particular the peak involving mainly the 0-0-0 vibrational transition, are weakened. In contrast if the signs differ, the 0-0-0 vibrational transition of $^1\Sigma^+_{0-}$ is greatly enhanced. One must notice that the intensity ratio between the 0-0-0 peak and ''0-0-1'' peak (actually continuum band) varies depending on the sign of the transition. The straightforward fitting procedure by using, e.g., Morse potentials thus may not be relevant and meaningful.

The interesting similarities between the adiabatic approximation of Fig. 4(a) and diabatic approximations in 4(c) and 4(d) appear in case of the transitions to higher bound states, which in the adiabatic picture can be associated to bound states of $^3\Pi_{0-}$. The similar states arise in the diabatic picture as well. It might be possible that these states may be recognized from an experimental spectrum measured with better statistics. As a conclusion the $^1\Sigma^+_{0-}$ and $^3\Pi_{0-}$ band profiles are very sensitive to the changes in the potential.

For the other dissociative states, like $4p\sigma^{-1}(^3\Pi_1)$ and $4p\sigma^{-1}\pi^{-1}(^1\Pi_1)$, the resulting vibrational band profiles can be predicted well by using more approximative methods, e.g. the moment method developed by Cederbaum and Tarantelli [19] and are not of specific interest to us.

IV. CONCLUSIONS

We have presented results of DHF and MR-RASCI calculations on the ground, Br $3d$–ionized, and doubly-valence-ionized states of HBr. Our results have been shown to be in overall agreement with recent experimental results [1]. The remaining inaccuracy in the calculations can be attributed to basis set effects and possibly to core-valence correlation effects. The results involving Br $3d$–ionized states must as well be considered preliminary, due to limitations of the CI method and the difficulties in obtaining the optimal starting vectors on DHF level. A more complete theoretical study of the Br $3d$ ionization is in our scope in the near future.

The vibrational band profiles of the resulting AES were studied in detail, and in particular it was found that the presence of avoided crossings caused by spin-orbit interaction may easily lead to situations where fitting procedures used in the data handling are not valid. First, the avoided level crossing leads to situations where transtions both to vibrational bound and continuum states are present simultaneously. Second, the intensity between various components of the vibrational bands may vary drastically because of strong spin-

orbit interaction. The distortion of the vibrational bands caused by lifetime vibrational interference was found to be of large importance.

Fully relativistic methods are shown to provide an effective tool to predict the energetics and vibrational structures of the molecules containing heavy element(s). The accuracy of the method compared to nonrelativistic treatment should be tested with some heavier molecule, e.g., HI, where the relativistic effects are expected to be even more pronounced also in the valence region.

ACKNOWLEDGMENTS

We thank R. Püttner and co-workers for putting the recent experimental results at our disposal prior to publication. T.M. thanks Odd Gropen for hospitality during the visit at the University of Tromsø. This work received support from The Research Council of Norway (Programme for Supercomputing) through a grant of computing time. Financial support from the Research Council for Natural Sciences of the Academy of Finland is acknowledged.

[1] R. Püttner, Y. F. Hu, G. M. Bancroft, H. Aksela, E. Nõmmiste, J. Karvonen, A. Kivimäki, and S. Aksela, Phys. Rev. A **59**, 4438 (1999).
[2] K. Ellingsen, T. Saue, H. Aksela, and O. Gropen, Phys. Rev. A **55**, 2743 (1997).
[3] E. Pahl, H. -D. Meyer, L. S. Cederbaum, D. Minelli, and F. Tarantelli, J. Chem. Phys. **105**, 9175 (1996).
[4] F. Gel'mukhnanov and H. Ågren, Phys. Rep. **312**, 87 (1999).
[5] A. Banichevich, S. D. Peyerimhoff, B. A. Hess, and M. C. van Hemert, Chem. Phys. **154**, 199 (1991).
[6] L. Visscher, O. Visser, P. J. C. Aerts, H. Merenga, and W. C. Nieuwpoort, Comput. Phys. Commun. **81**, 120 (1994). See also http://theochem.chem.rug.nl/~bert/Molfdir/Molfdir.html
[7] J. Olsen, B. O. Roos, P. Jørgensen, and H. J. Aa. Jensen, J. Chem. Phys. **89**, 2185 (1988).
[8] K. Fægri (private communication).
[9] T. H. Dunning, Jr., J. Chem. Phys. **90**, 1007 (1989).
[10] L. Visscher, P. J. C. Aerts, O. Visser, and W. C. Nieuwpoort, Int. J. Quantum Chem., Quantum Chem. Symp. **25**, 131 (1991).
[11] W. Wannberg, S. Svensson, M. P. Keane, L. Karlsson, and P. Balzer, Chem. Phys. **133**, 281 (1989).
[12] K. P. Huber and G. Herzberg, *Constants of Diatomic Molecules* (Van Nostrand Reinhold, New York, 1979).
[13] Y. F. Hu, Z. F. Liu, R. Püttner, G. M. Bancroft, and S. Aksela J. Phys. B **32**, 4031 (1999).
[14] R. Püttner, M. Domke, K. Schulz, and G. Kaindl, J. Phys. B **28**, 2425 (1995).
[15] L. Visscher, J. Styszyñski, and W. C. Nieuwpoort, J. Chem. Phys. **105**, 1987 (1996).
[16] S. R. Langhoff and E. R. Davidson, Int. J. Quantum Chem. **8**, 61 (1974).
[17] N. Correia, A. Flores-Riveros, H. Ågren, K. Helenelund, L. Asplund, and U. Gelius, J. Chem. Phys. **83**, 2035 (1985).
[18] K. G. Dyall, J. Chem. Phys. **100**, 2118 (1994).
[19] L. S. Cederbaum and F. Tarantelli, J. Chem. Phys. **98**, 9691 (1993).